annealing runs. Over the entire range of stress levels considered, we consistently observe a smaller $\lambda^{\max}$ for $\boldsymbol{\beta}_{\neq}$ compared to $\boldsymbol{\beta}_{=}$, the optimal homogeneous β_i assignment, and to $\boldsymbol{\beta}_0$, the original β_i assignment in the dataset (Fig. 4a).

To test the robustness of the identified optimal $\lambda^{\max}$ against uncertainties in the β_i values, we study how $\lambda^{\max}$ changes under perturbations along random directions in the $\boldsymbol{\beta}$-space in the vicinity of $\boldsymbol{\beta}_{\neq}$ and (for comparison) in the vicinity of $\boldsymbol{\beta}_{=}$. For the stress level of 1 and for each random direction, we compute $\lambda^{\max}$ as a function of the perturbation size ε, measured in 2-norm. The resulting statistics from 1,000 random directions indicate that, for each system, there is a sizable neighborhood of the optimum $\boldsymbol{\beta}_{\neq}$ in which $\lambda^{\max}$ is significantly lower than at $\boldsymbol{\beta}_{=}$, representing a stability improvement against small perturbations (Fig. 4b).

To show that the improvement is also observed for stability against large perturbations, we define a generalized notion of attraction basin as a set of initial conditions whose corresponding trajectories satisfy a criterion for convergence to synchronous states (a variation of the so-called basin stability[28]). Here, the convergence criterion we use is that the instantaneous frequency enters into a narrow band around ω_{s} (within ± 0.3 Hz) and remains inside the band until $t_{\max} = 10$ seconds. This criterion is similar to what is typically used for transient stability analysis in power system engineering. It also captures a variety of synchronous states, including not only those corresponding to fixed points of Eq. (1) (with constant phase angle differences), but also those corresponding to time-dependent solutions of Eq. (1). To account for large perturbations, we consider initial conditions with arbitrary phase angles and frequencies within 1 Hz of the nominal frequency (60 Hz for the New England and NPCC systems; 50 Hz for the U.K. and German systems). Each initial condition can be regarded as resulting from a large impulse-like disturbance, such as a disconnection of a significant portion of the grid or a system-wide demand surge. The size of the basin can then be quantified using the fraction f of the corresponding trajectories that converge before a given cutoff time t_c, i.e., the fraction of those that satisfy $|\dot{\delta}_i(t)|/(2\pi) \leq 0.3$ Hz for all $t \in [t_c, t_{\max}]$. For each t_c, the fraction f is estimated using 1,000 initial conditions sampled randomly and uniformly from all states satisfying the criteria described above. As shown in Fig. 4c, we find that the estimated f is significantly larger for $\boldsymbol{\beta}_{\neq}$ than for $\boldsymbol{\beta}_{=}$ (which in turn is much larger than for $\boldsymbol{\beta}_0$). This indicates that the likelihood for the system to return to stable operation after a large disturbance is higher for the heterogeneous optimal β_i than for the homogeneous optimal ones. We also observe that larger systems tend to exhibit larger increase in the size of the asymptotic basins (i.e., in the value of f for $t_c \to \infty$).

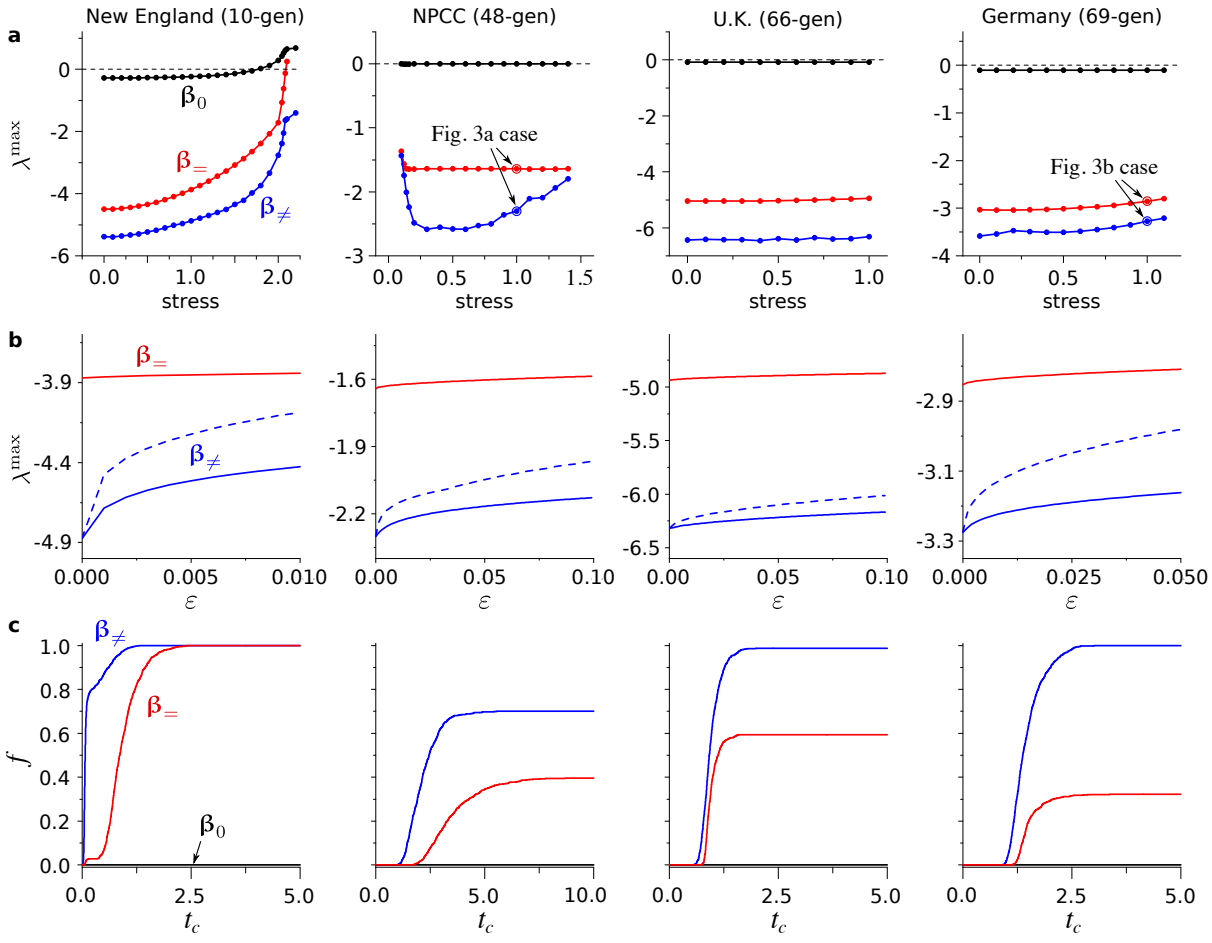

Fig. 4: **Improving the stability of power grids with heterogeneity in β.** The columns correspond to the four systems we consider. **a** Improved Lyapunov exponent $\lambda^{\max}$ as functions of the system stress level for the heterogeneous optimum $\boldsymbol{\beta}_{\neq}$ (blue), the homogeneous optimum $\boldsymbol{\beta}_{=}$ (red), and the original parameter $\boldsymbol{\beta}_0$ (black). The cases shown in Fig. 3 are indicated in the second and the last plot. **b** Change of $\lambda^{\max}$ under perturbations of size ε applied to $\boldsymbol{\beta}_{\neq}$ (blue). We show $\lambda^{\max}$ as a function of ε, where solid and dashed curves indicate the average and the maximum, respectively, over perturbations in 1,000 random directions. Note that the maximum corresponds to the worst case scenario. For comparison, we also show the average of $\lambda^{\max}$ when $\boldsymbol{\beta}_{=}$ is perturbed (red). **c** Fraction f of trajectories that converge to synchronous states before a given cutoff time t_c for $\boldsymbol{\beta}_{\neq}$ (blue), $\boldsymbol{\beta}_{=}$ (red), and $\boldsymbol{\beta}_0$ (black). Note that f for $\boldsymbol{\beta}_0$ remains zero for all $t_c < 10$ seconds in all cases.

Isolating converse symmetry breaking. Since real power systems generally have heterogeneity in a_i, c_{ik}, and γ_{ik}, the stability improvement enabled by the β_i heterogeneity (and the associated system asymmetry) could in principle be a compensation for heterogeneity in the network structure, power demand and generation, or other component parameters (and the associated system asymmetries). To illustrate that no such compensation is needed and that CSB can be responsible for stability improvement, we use an example system consisting of four generators connected to each other and to one load (see Supplementary Fig. 1 for a system diagram). This system is symmetric with respect to the permutation of generators 2 and 3 if $\beta_2 = \beta_3$, and this symmetry is reflected in the property that $P_{2j} = P_{3j}$ for all j in the corresponding interaction matrix $\mathbf{P}$ (Fig. 5a). The minimum $\lambda^{\max}$ possible for this symmetric system is $\lambda^{\max} \approx -2.40$, which can be decreased further by more than 20% to $\lambda^{\max} \approx -2.97$ if the $\beta_2 = \beta_3$ constraint is lifted (Fig. 5b–d). This demonstrates CSB for this system under a range of noise levels: breaking the system's symmetry under the permutation of generators 2 and 3 is required for $\lambda^{\max}$ to cross the stability threshold and make the (symmetric) synchronous state stable. We note that the observation of CSB depends on the system's symmetry. While CSB is observed in this 4-generator system (with a two-generator permutation symmetry), we do not observe CSB in a variant of the system with the four-generator permutation symmetry. We also note that, while the optimal β_i assignment does not share the two-generator permutation of the system, the two-dimensional stability landscape does, and it features a pair of equally optimal assignments related to each other through the symmetry (Fig. 5b). It is instructive to compare this result with the mass-spring system in Fig. 1, where similar breaking of a permutation symmetry (between masses 1 and 3) for a symmetric landscape (where optimal b_1 and b_3 are necessarily different but can be swapped) is shown to underlie optimal damping.

Having established that β_i heterogeneity alone can enhance stability through CSB, we now introduce a systematic method to separate CSB from other mechanisms that involve interplays between multiple heterogeneities. For this purpose, we transform matrix $\mathbf{P}$ for each system used in Fig. 4, which does not have a pairwise node permutation symmetry, to a slightly different matrix $\mathbf{P}'$ that does have the symmetry. More precisely, for a given pair of nodes i_1 and i_2, we define this symmetrized matrix $\mathbf{P}'$ by $P'_{i_1 j} = P'_{i_2 j} \equiv (P_{i_1 j} + P_{i_2 j})/2$ for all $j \neq i_1$ nor i_2, making it symmetric under the permutation of nodes i_1 and i_2. To elucidate CSB for each system, we chose a node pair that simultaneously minimizes the difference between $\mathbf{P}$ and $\mathbf{P}'$ and maximizes the amount of stability improvement observed for $\mathbf{P}'$. For the four systems in Fig. 4, the stability of the symmetrized system can clearly be enhanced by allowing $\beta_{i_1} \neq \beta_{i_2}$,